2.25MHz offset. The developed device meets the IS-95 CDMA device specifications under both 3.0V and 2.4V bias conditions.

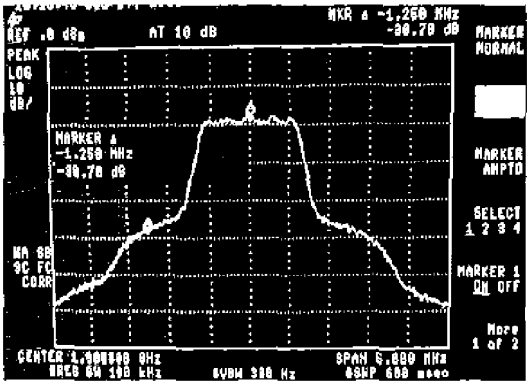

566/4

Fig. 4 *CDMA spectrum of 20.16mm device at 3.0V drain bias voltage*

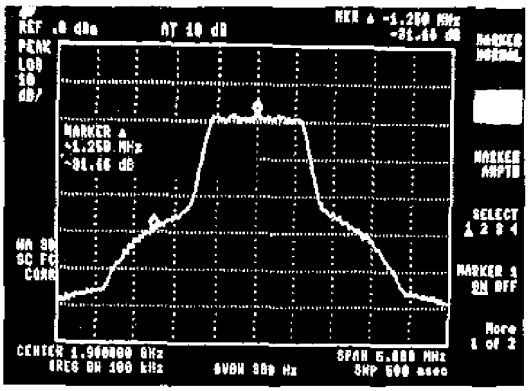

566/5

Fig. 5 *CDMA spectrum of 20.16mm device at 2.4V drain bias voltage*

Conclusions: A low voltage power PHEMT for CDMA applications has been developed. The device has a double delta-doped AlGaAs/InGaAs/GaAs structure to provide high drain current density and transconductance. The size of the layout of the device was reduced to improve the low the voltage performance. At 2.4V bias, the developed device shows an output power of 30dBm with a power added efficiency of 61.5% and the gain of the device at maximum output power is 8.47dB. When tested under IS-95 CDMA modulation conditions, the device meets the CDMA specifications at both 3.0V and 2.4V drain bias. At 28dBm linear output power for CDMA application, the device has a power added efficiency of 37.8% at 3.0V bias and 30.2% at 2.4V bias. This Letter represents the first report on power PHEMTs for 2.4V CDMA applications. The device should be applicable to the next generation of digital wireless communication systems.

Acknowledgment: This work was supported in part by the National Science Council of the Republic of China under Contract NSC-89-2213-E-009-047.

25 January 2000

Electronics Letters Online No: 20000360

DOI: 10.1049/el:20000360

E.Y. Chang, Di-Hoong Lee, S.H. Chen and H.C. Chang (*Department of Materials Science and Engineering and Institute of Materials Science and Engineering, National Chiao Tung University, Hsinchu, 300, Taiwan, Republic of China*)

E-mail: edc.cc.nctu.edu.tw

References

1 LAI, YEONG-LIN, CHANG, EDWARD Y., CHANG, CHUN-YEN, CHEN, T.K., LIU, T.H., WANG, S.P., CHEN, T.H., and LEE, C.P.: '5mm high-power-density dual-delta-doped power HEMT's for 3V L-band application', *IEEE Electron Device Lett.*, 1996, **17**, (5), pp. 229–231

2 LAI, YEONG-LIN, CHANG, EDWARD Y., CHANG, CHUN-YEN, LIU, T.H., WANG, S.P., and HSU, H.T.: '2-V-operation δ-doped power HEMT's for personal handy-phone system', *IEEE Microw. Guid. Wave Lett.*, 1997, **7**, (8), pp. 219–221

3 WANG, Y.C., KUO, J.M., LOTHIAN, J.R., REN, F., TSAI, H.S., WEINER, J.S., LIN, J., TATE, A., MAYO, W.E., and CHEN, Y.K.: 'High efficiency $In_{0.3}(Al_{0.3}Ga_{0.7})_{0.5}P/In_{0.2}Ga_{0.8}As$ power HEMT for low supply voltage wireless communications'. 55th Annual Device Research Conf. Dig., New York, 1997, pp. 70–71

4 MARTINEZ, M.J., SCHIRMANN, E., DURLAM, M., HUANG, J.H., TEHRANI, S., CODY, N., DRIVER, T., and BARKLEY, K.: 'AlGaAs/InGaAs power P-HEMTs for high-efficiency, low-voltage portable applications'. IEEE MTT-S Int. Microw. Symp. Dig., 1996, pp. 551–553

5 IWATA, N., YAMAGUCHI, K., NISHIMURA, T.R., TAKEMURA, K., and MIYASAKA, Y.: '49% efficiency power amplifier MMIC utilizing SrTiO3 capacitors for 3.5V Li-ion battery operated CDMA cellular phones'. IEEE RFIC Symp. Tech. Dig., New York, 1998, pp. 65–68

Reduction of epitaxial alignment in n^+-p poly-Si emitter diode due to gettering of P and As by Ar implantation

Lurng Shehng Lee and Chung Len Lee

It is demonstrated that Ar implantation can retard the epitaxial realignment of poly-Si/Si in an As- or P-doped n^+-p poly-emitter diode during BF_2 implantation. This is believed to be due to the gettering of As, P, and F by bubble-like defects created by the Ar implantation used to reduce the pile-up of these dopants at the poly-Si/Si interface. Consequently, there is less break-up of the interface oxide, resulting in a reduction in epitaxial realignment.

Introduction: The use of a highly-doped poly-Si film as the diffusion source to form a shallow emitter has been widely adopted for fabricating high performance bipolar transistors [1, 2]. However, the high emitter drive-in thermal budget induces epitaxial realignment of the polysilicon [3]. In particular, the incorporated-F in the polysilicon, which is present due to the BF_2 ion implantation, enhances oxide break-up, causing more epitaxial realignment of the polysilicon [4, 5]. This epitaxial realignment results in an extended single crystal emitter, degrading the current gain of the transistor [6].

It was proposed and demonstrated that Ar implantation could be used to suppress the boron penetration in p^+ PMOSFETs [7]. It is expected that this technique can be applied to the double-diffused n^+/p poly-Si emitter diode to suppress the epitaxial realignment. In this Letter, it is demonstrated that this technique enables the achievement of this goal.

Experiment: In this experiment, the n^+-p poly-Si diodes were fabricated on p-type 15 25Ωcm (100) Si wafers. First, all wafers were dipped in an $HF:H_2O$ (1:10) solution to remove the native surface oxide. A poly-Si film of 3000Å was then deposited at 620°C, followed by an Ar implantation dose of $10^{16}cm^{-2}$ at 80keV. The projected range of the Ar was ~900Å. An As or P dose of $2 \times 10^{16}cm^{-2}$ was then implanted in the wafers at 80keV. BF_2 implantation with a dose of $4 \times 10^{15}cm^{-2}$ at 60keV was then carried out to simulate an emitter transistor structure with an extrinsic base. After all implantations, a 90Å oxide layer was grown on the wafers to prevent impurity out-diffusion, and then the wafers were annealed in a furnace in N_2 ambient at 900°C for 60min. All the wafers then received an additional rapid thermal annealing (RTA) at 1100°C for 20s in N_2 ambient. For comparison, similar devices without Ar implantation were also fabricated.

Results and discussion: Fig. 1*a* and *b* show the TEM cross-sectional micrographs of the junction region of the poly-Si emitter

contacted n^+-p diodes without and with Ar implantation, respectively. For the diode without Ar implantation in Fig. 1*a*, the poly-Si/Si interface was fully broken and complete epitaxial realignment of the poly-Si with respect to the Si substrate was observed. This is consistent with the result reported in [6]. However, for the diode with Ar implantation (Fig. 1*b*), only half of the poly-Si was epitaxially realigned (region B of the micrograph). The associated TEM diffraction patterns of regions A and B are also shown in Fig. 1*b*. These patterns indicate that region A is polycrystalline and region B is a mono-crystal. Fig. 2 shows an enlarged TEM micrograph of region A, where bubble-like defects in the

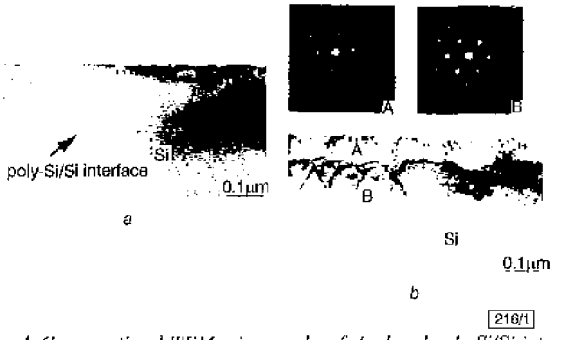

Fig. 1 *Cross-sectional TEM micrographs of As-doped poly-Si/Si interface of samples*

a Without Ar
b With Ar implantation
Diffraction patterns of regions A and B are also shown in Fig. 1*b*

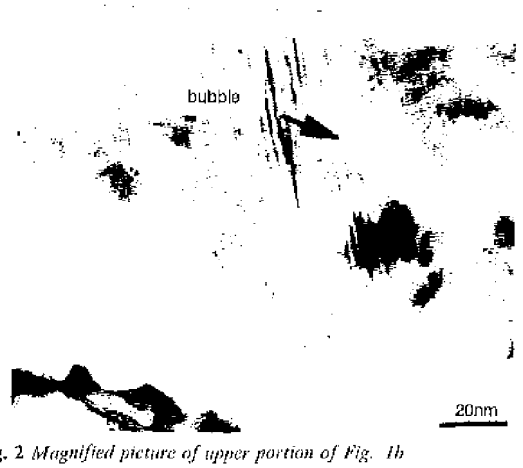

Fig. 2 *Magnified picture of upper portion of Fig. 1b*

Bubbles due to Ar implantation are observed

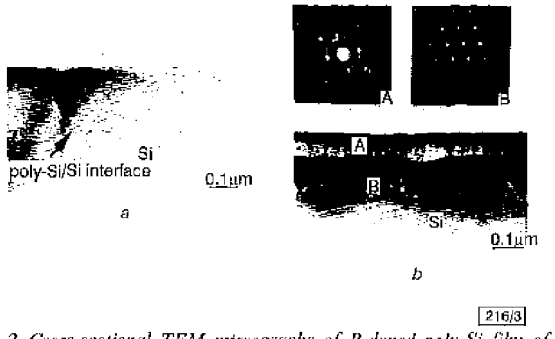

Fig. 3 *Cross-sectional TEM micrographs of P-doped poly-Si film of samples*

a Without Ar implantation
b With Ar implantation
Diffraction patterns of regions A and B are also shown in Fig. 3*b*

implanted polycrystal line region can be observed. These bubble-like defects are believed to act as gettering centres for As, B and F atoms, retarding their diffusion into the poly-Si/Si interface. Fig. 3*a* and *b* show similar TEM micrographs of the diodes which were implanted with P instead of As. For the diode without Ar implantation (Fig. 3*a*), the poly-Si/Si interface was also fully broken and complete epitaxial realignment of the poly-Si occurred, but for the diode with Ar implantation (Fig. 3*b*), only half of the poly-Si emitter was epitaxially realigned (region B). For this sample, however, more micro-twins than those of the As–doped diode of Fig. 1*b* are observed. The associated TEM diffraction patterns of regions A and B for this diode are also included in Fig. 3*b*. They also indicate that region A was polycrystalline and region B was a single crystal.

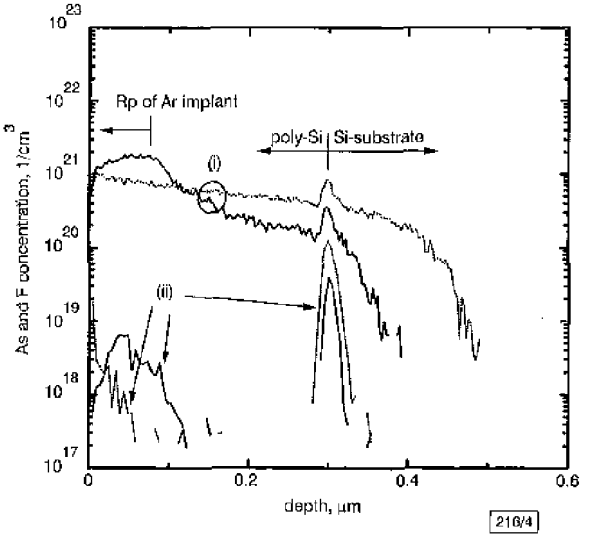

Fig. 4 *SIMS profiles of As and F of n^+-p polyemitter samples of Fig. 1a and b*

(i) As
(ii) F
—— with Ar implantation, 10^{16}cm^{-2}
····· without Ar implantation

Fig. 4 shows the secondary ion mass spectrometry (SIMS) profiles of As and F, respectively, of the n^+-p poly-emitters of Fig. 1*a* and *b*. It can also be seen that the Ar implanted sample had higher As and F peaks at the Rp of the implanted Ar in the poly-Si film, a lower F peak at the poly-Si/Si interface and a shallower As profile in the underlying silicon substrate. The lower As and F concentration resulted in a lower level of epitaxial realignment of the poly-Si with respect to the Si substrate. A similar SIMS profile of P and F for the n^+-p poly-emitter diode of Fig. 3 showed the same result.

Conclusion: In this Letter, it has been demonstrated that Ar implantation can retard the epitaxial realignment in an n^+-p poly-emitter diode by creating bubble-like defects which getter F, As, and P. This technique could be useful for improving the gain of the poly-emitter transistor in bipolar ICs.

28 December 1999
Electronics Letters Online No: 20000379
DOI: 10.1049/el:20000379

Lurng Shehng Lee and Chung Len Lee (*Department of Electronics Engineering and Institute of Electronics, National Chiao Tung University, Hsinchu, Taiwan, Republic of China*)

Lurng Shehng Lee: also with ERSO/ITRI, Hsinchu, Taiwan, Republic of China

References

1 NING, T.H., and ISAAC, R.D.: 'Effect of emitter contact on current gain of silicon bipolar devices', *IEEE Trans. Electron Devices*, 1980, **ED-27**, pp. 2051–2055

2 PATTON, G.L., BRAYMAN, J.C., and PLUMMER, J.D.: 'Physics, technology, and modeling of polysilicon emitter contacts for VLSI bipolar transistors', *IEEE Trans. Electron Devices*, 1986, **ED-33**, pp. 1754–1768

3 AJURIA, S.A., and REIF, R.: 'Early stage evolution kinetics of the polysilicon/single-crystal silicon interfacial oxide upon annealing', *J. Appl. Phys.*, 1991, **69**, pp. 662–667
4 WU, S.L., LEE, C.L., LEI, T.F., CHEN, C.F., CHEN, L.J., HO, K.Z., and LING, Y.C.: 'Enhancement of oxide break-up by implantation of fluorine in poly-Si contacted p⁺-n shallow junction formation', *IEEE Electron Device Lett.*, 1994, **15**, pp. 120–122
5 GRAVIER, T., KRITSCH, I., D'ANTERROCHES, C., and CHANTRE, A.: 'Fluorine effects in n-p-n double-diffused polysilicon emitter bipolar transistors', *IEEE Electron Device Lett.*, 1996, **17**, pp. 434–436
6 BURK, D.E., and YUNG, S.-Y.: 'Experimental verification of the extentended-concept for phosphorus-implanted self-aligned polysilicon-contacted bipolar transistors', *Solid-State Electron.*, 1988, **31**, pp. 1127–1138
7 LEE, L.S., and LEE, C.L.: 'Argon ion-implantation on polysilicon or amorphous-silicon for boron penetration suppression in p⁺ PMOSFET', *IEEE Trans. Electron Devices*, 1998, **49**, pp. 1737–1744

Denoising by optimal fuzzy thresholding in wavelet domain

L.-K. Shark and C. Yu

The construction of a hybrid wavelet threshold is presented based on fuzzy combination of an unbiased risk estimate and an asymptotic near-minimax fixed threshold for noise suppression. The optimality of the proposed threshold is demonstrated by recovering a Gaussian envelope sinusoidal signal embedded in the additive white Gaussian noise in good and poor signal-to-noise ratio scenarios.

Introduction: In denoising based on the discrete wavelet transform (DWT), the general approach is to apply a threshold to the wavelet coefficients produced by the forward DWT of the noise-corrupted signal, thereby allowing only significant wavelet coefficients with their magnitude values greater than the threshold to be used in the inverse DWT (IDWT) to reconstruct the original signal. Consequently, there exists a dilemma in setting an appropriate threshold: raising the threshold to reduce the noise contribution in signal reconstruction can increase the signal distortion, because it may result in small wavelet coefficients due to the signal being excluded in the IDWT; alternatively, lowering the threshold to increase the signal contribution in signal reconstruction can increase noise interference, because it may result in small wavelet coefficients due to noise being included in the IDWT. To solve the dilemma, a special fuzzy membership function has been previously proposed such that the contribution of a wavelet coefficient in signal reconstruction depends on the relative significance of its magnitude value [1]. However, the computation of the optimal fuzzy membership function requires knowledge of the signal to be recovered. To extend fuzzy thresholding to the recovery of unknown signals, this Letter presents the construction of a level-dependent optimal fuzzy membership function by combining Stein's unbiased risk estimate (SURE) and an asymptotic near-minimax fixed threshold to determine the best values for its controlling parameters. Also presented are the computer simulation results to demonstrate the optimality of the proposed fuzzy thresholding function for denoising.

Optimal fuzzy thresholding: If s_n is the signal to be restored and w_n is the additive zero mean white Gaussian noise with variance σ^2, then the received signal is given by

$$r_n = s_n + w_n \qquad n = 0, 1, ..., N-1 \tag{1}$$

where N is the number of samples in the received signal. Applying the DWT with M decomposition stages to r_n yields an approximation coefficient sequence at the coarsest resolution, $a_{M,n}$, with $n = 0, 1, ..., (N/2^M) - 1$, and a set of detail coefficient sequences at different resolutions, $d_{m,n}$, with $m = 1, 2, ..., M$ and $n = 0, 1, ..., (N/2^m)-1$. Since the DWT is a linear operation, the DWT of the received signal can be viewed as a linear superposition of the DWT of s_n with a small number of significant coefficients and the DWT of w_n with a large number of small coefficients. Consequently, denoising becomes a problem of formulating an appropriate threshold to exclude small detail coefficients (presumably generated by noise) in the IDWT, thereby yielding a restored version of the original signal, $\hat{s}_n$.

A fixed form threshold with some asymptotic near-minimax properties for the detail coefficients at the mth resolution level is given by [2]

$$t_m^{fixed} = \hat{\sigma}\sqrt{2\ln\left(\frac{N}{2^m}\right)} \tag{2}$$

where $\hat{\sigma}^2$ is the noise variance estimated using the detail coefficients at the first resolution level as

$$\hat{\sigma} = \frac{\text{median}|d_{1,n}|}{0.6745} \tag{3}$$

Although this choice of threshold value is simple, it is known as a conservative one that tends to zero out more detail coefficients as the number of detail coefficients increases. At the limit, the probability of a detail coefficient at the mth resolution level having a value greater than t_m^{fixed} will tend to zero as N approaches ∞.

An alternative choice for yielding a lower threshold value came from the Stein unbiased risk estimate (SURE) based on minimisation of the mean-squared errors between s_n and $\hat{s}_n$ by varying the threshold t from zero up to t_m^{fixed} [3]

$$t_m^{sure} = \underset{0 \le t \le t_m^{fixed}}{\text{argmin}} \left[\frac{\hat{\sigma}^2 N}{2^m} + \sum_{n=0}^{\frac{N}{2^m}-1} \{d_{m,n}^2 \wedge t^2\} - 2\hat{\sigma}^2 \#\{|d_{m,n}| \le t\} \right] \tag{4}$$

where $\#\{|d_{m,n}| \le t\}$ denotes the number of detail coefficients having magnitude values less than t. Compared with the fixed form threshold, the behaviour of the SURE threshold tends to be erratic and tends to include more detail coefficients in signal reconstruction as the noise contribution increases.

Consequently, there is a problem in selecting between the fixed form threshold and the SURE threshold. While the former can be viewed as the upper bound because it tends to 'overkill' the detail coefficients, the latter can be viewed as the lower bound because it tends to 'underkill' the detail coefficients. A possible compromise is to use a fuzzy membership function to allow the detail coefficients lying between t_m^{fixed} and t_m^{sure} to contribute partially in the signal reconstruction according to their magnitude values (proportional shrinkage of the detail coefficients). One particular membership function, which was found to perform well for signal recovery using the DWT, is given by [1]

$$\mu_F(d_{m,n}) = 1 - \frac{\mu(d_{m,n})}{\max\{\mu(d_{m,n})\}} \tag{5}$$

where

$$\mu(d_{m,n}) = \frac{b_m}{b_m + \exp(c_m d_{m,n}^M) + \exp(-c_m d_{m,n}^M)} \tag{6}$$

and where b_m and c_m are parameters controlling the transition of the s-shape membership function. It should be apparent from eqns. 5 and 6 that, as $d_{m,n}$ approaches zero, $\mu(d_{m,n})$ approaches $\max\{\mu(d_{m,n})\} = b_m/(b_m+2)$, and $\mu_F(d_{m,n})$ approaches the membership value of zero. Conversely, as $d_{m,n}$ increases, $\mu(d_{m,n})$ decreases, and $\mu_F(d_{m,n})$ approaches the membership value of 1.

The best values for b_m and c_m can be determined by assigning appropriate values for the membership function at the lower bound t_m^{sure} and the upper bound t_m^{fixed}. Since the detail coefficients with values less than t_m^{sure} are most likely to be produced by noise, it is reasonable to set the membership value to almost zero, denoted by Δ, when the detail coefficients equal t_m^{sure}. Substituting t_m^{sure} and Δ in eqn. 5 gives

$$\frac{\exp\left[c_m\left(t_m^{sure}\right)^4\right] + \exp\left[-c_m\left(t_m^{sure}\right)^4\right] - 2}{b_m + \exp\left[c_m\left(t_m^{sure}\right)^4\right] + \exp\left[-c_m\left(t_m^{sure}\right)^4\right]} = \Delta \tag{7}$$

Similarly, since the detail coefficients with values greater than t_m^{fixed} are most likely to be produced by the original signal, it is reasonable to set the membership value to almost one, denoted by $1-\Delta$, when the detail coefficients equal t_m^{fixed}. Substituting t_m^{fixed} and $1-\Delta$ into eqn. 5 gives